

## ORIGINAL ARTICLE

## Multinucleation of koilocytes is in fact multilobation and is related to aberration of the G2 checkpoint

N H Cho, S Kang, S Hong, G B Jeong, I W Choi, H J Choi, H K Choi

*J Clin Pathol* 2005;58:576–582. doi: 10.1136/jcp.2004.022152

See end of article for authors' affiliations

Correspondence to:  
Dr N H Cho, Department  
of Pathology,  
Seodaemun-ku, Sinchon-  
dong 134, Yonsei  
University College of  
Medicine 120-752, Seoul,  
Korea; cho1988@yumc.  
yonsei.ac.kr

Accepted for publication  
28 October 2004

**Aims:** To clarify the fine structure of koilocytes and correlate this with genetic aberration of the G2 checkpoint

**Methods:** Three dimensional reconstruction from confocal fluorescent images, together with functional assays for key molecules of the G2 checkpoint—cdc2 and cyclin B1—was performed in human uterine cervical samples. After confirming 22 human papillomavirus (HPV) types using a DNA chip from 30 cervical swabs, previously confirmed as 15 cervical low grade and 15 high grade intraepithelial lesions, the activity of molecules involved in the G2 checkpoint was evaluated using western blotting for cyclin B1, cdc2, and phospho-cdc2 (Y15 and T161), a nuclear extraction fractional assay, and a reverse transcription polymerase chain reaction assay. In addition, three dimensional confocal image restoration was performed on confirmed cervical intraepithelial neoplasia tissue samples.

**Results:** T161 phospho-cdc2 and cyclin B1 expression was higher in HPV infected cervical lesions than in normal samples. Immunofluorescence, revealed that cyclin B1 was present predominantly in the nuclei of HPV infected cells, confirming the results of the nuclear fractional assay. On restoration of three dimensional confocal images, the multinucleation of koilocytes was revealed to be multilobation of a single nucleus, rather than true multinucleation. This multilobation appeared to be associated with chromosomal instability and aberration of the G2 checkpoint.

**Conclusions:** The multiple nuclei of koilocytes are in fact multilobation of a single nucleus, and this phenomenon is associated with upregulation of gene products related to the G2 checkpoint.

Koilocytes are defined as squamous cells with a large, well demarcated, clear perinuclear zone surrounded by a dense peripheral cytoplasmic rim. These changes predominantly affect superficial and intermediate cells, and provide the most reliable evidence of human papillomavirus (HPV) infection.<sup>1,2</sup> One of the most distinctive features of koilocytes is multinucleation, which is not specific for HPV infection, and be seen in reactive processes, including post-irradiation reactivity.<sup>2</sup> Nevertheless, the presence of koilocytes is a common feature in HPV infection, adding weight to the diagnosis, especially when extensive. However, it is doubtful whether virally infected keratinocytes are truly multinucleated even in when the G2 checkpoint is aberrant.

HPV genomes are established as episomes at approximately 50 copies/cell after infection of keratinocytes in the basal layer, and they replicate in synchrony with cellular DNA replication.<sup>3,4</sup> In contrast to normal differentiating suprabasal cells, which exit the cell cycle, HPV infected cells remain active in the cell cycle and re-enter S phase until they reach terminal differentiation, resulting in amplification of the viral E1 and E2 genes and expression of late transcripts in a differentiation dependent manner.<sup>5-7</sup> The mammalian cell division cycle is governed by the orchestrated activation and inactivation of cyclin dependent kinases (cdks).<sup>3</sup> During the G1 phase, cyclins D1, D2, and D3 form complexes with cdk4 and cdk6, and cyclin E with cdk2; these complexes function as retinoblastoma kinases, and modulate the activity of E<sub>2</sub>F, hence modulating the expression of proliferative genes. Cyclin A associates with cdk2 during the S phase, and with cdc2 (cdk1) at the S–G2 boundary and into G2. Progression through G2, culminating in mitosis, requires cdc2 to form complexes with cyclin B1 and B2. Threonine residue 161 of mammalian cdc2 is implicated in cyclin binding, and phosphorylation at this position may be a prerequisite for the association between cdc2 and cyclin B1.<sup>8,9</sup> The cyclin B–

cdc2 complex accumulates in G2, and is negatively regulated before mitosis by phosphorylation at threonine 14 (T14) and tyrosine 15 (Y15) of cdc2. Dephosphorylation of both residues (T14 and Y15) is required for the activation of cyclin B–cdc2, and a dual specific phosphatase, cdc25, carries out this dephosphorylation. G2 checkpoint aberrations may directly result in abnormal centrosome numbers—aneuploidy—and may lead to genomic instability.<sup>10-14</sup> High risk HPV E6/E7 oncoproteins cooperate to induce centrosome abnormality and mitotic defects, which accumulate in parallel with nuclear atypia, predominantly multinucleation.<sup>13</sup> Expression of either E6 or E7 can independently bypass the mitotic checkpoint. E6 can inhibit the checkpoint by degradation of p53, whereas E7 appears to bypass the checkpoint in the presence of high concentrations of p53, possibly through the loss of the retinoblastoma protein and/or the increased expression of the cellular oncoprotein MDM2 (mouse double minute 2).<sup>14</sup>

“The mammalian cell division cycle is governed by the orchestrated activation and inactivation of cyclin dependent kinases”

We aimed to clarify the fine structure of koilocytes and to correlate their presence with genetic aberrations of the G2 checkpoint at the transcriptional and post-translational levels of the cyclin B1–cdc2 complex. We found that samples with HPV infection showed increased expression of T161-cdc2 and cyclin B1. Using three dimensional confocal reconstruction

**Abbreviations:** cdk, cyclin dependent kinase; HPV, human papillomavirus; HSIL, high grade squamous intraepithelial lesion; PBS, phosphate buffered saline; PCR, polymerase chain reaction; PI, propidium iodide; SSPE, saline sodium phosphate–EDTA buffer; RT, reverse transcription

analyses, we also found that the multiple nuclei of koilocytes are in fact the result of multilobation of one nucleus and that this phenomenon is associated with upregulation of gene products related to G2 checkpoint aberration in koilocytes, as assessed by the nuclear fractional assay and confocal double immunofluorescence.

## MATERIALS AND METHODS

Our study was conducted at an outpatient clinic of the Yonsei University College of Medicine in Seoul, Korea. We investigated 30 cervicovaginal swabs using conventional Papanicolaou smears and simultaneously performed HPV genotyping analysis by DNA chip microarray, followed by L1 consensus polymerase chain reaction (PCR). We used 15 cervical swabs from the "within normal limits" category as the control group.

After confirmation of 22 HPV genotypes by DNA chip (Biomed Lab Co, Seoul, Korea), we looked at koilocytes from the cervical swab and tissue specimens by three dimensional confocal restoration—we reconstructed stacks of two dimensional images of koilocytes to produce three dimensional images by confocal microscopy. We evaluated the functional activity of the G2 molecules in 30 cervical swabs by western blotting for cyclin B1, cdc2, and phospho-cdc2 (Y15), compared the relative amounts of G2 checkpoint molecules in the nuclei and the cytoplasm using the nuclear fractional assay, and analysed transcript levels by reverse transcription (RT) PCR. Furthermore, we performed indirect immunofluorescence for cyclin B1 and cdc2 in 30 paraffin wax embedded cervical intraepithelial lesion samples corresponding to the cervical swab samples.

## HPV genotyping

HPV detection and genotyping were performed using an HPVDNAChip and a PCR based DNA microarray system provided by Microarray Centre, Biomed Lab Co. The HPVDNAChip contains 22 type specific probes that consist of 15 high risk groups (16, 18, 31, 33, 35, 39, 45, 51, 52, 56, 58, 59, 66, 68, and 69) and seven low risk groups (6, 11, 34, 40, 42, 43, and 44). DNA was isolated from swab samples using a DNA isolation kit (Qiagen, Hilden, Germany), and target HPV DNA was amplified by PCR using GP5d+/GP6d+ primers (GP5d+, 5'-TTTCTTACHGKTGTDGATACYAC-3'; GP6d+, 5'-GAAAHATAAAAYTGYAADTCATAYTC-3'; K, G/T; H, T/A/C; D, A/T/G; Y, T/C).  $\beta$  Globin was PCR amplified with the PC03/PC04 primers (PC03, 5'-ACACAACCTGTGTTCACTAGC-3'; PC04, 5'-CAACTTCATCCACGTTACC-3') as an internal control. Amplified DNA was labelled by Cy5-dUTP (NEN; Life Science Products Inc, Boston, Massachusetts,

USA). HPV amplified products and  $\beta$  globin amplified products were denatured by incubating with 3N sodium hydroxide solution (10% vol/vol) at room temperature for five minutes, neutralised by adding 1 mol/litre Tris/HCl (pH 7.2; 5% vol/vol) then 3N hydrochloric acid (10% vol/vol), and finally cooled for five minutes on ice. The cervical samples were mixed with a hybridisation solution made of 6  $\mu$ l SSPE (saline sodium phosphate-EDTA buffer; Sigma Chemical Co, St Louis, Missouri, USA) and 0.2% sodium dodecyl sulfate and applied to the DNA chip. Hybridisation was performed at 40°C for two hours and the samples were then washed with 3  $\mu$ l SSPE for two minutes, 1  $\mu$ l SSPE for two minutes, and air dried at room temperature. Hybridised HPV DNA was visualised using a DNA chip scanner (ScanArray Lite; GSI Lumonics, Ottawa, Canada).

## Western blotting

Cervical swabs were washed twice in cold phosphate buffered saline (PBS) and lysed in lysis buffer (50mM Tris/HCl, pH 7.5; 120mM NaCl; 5% Nonidet P400; 10mM NaF;

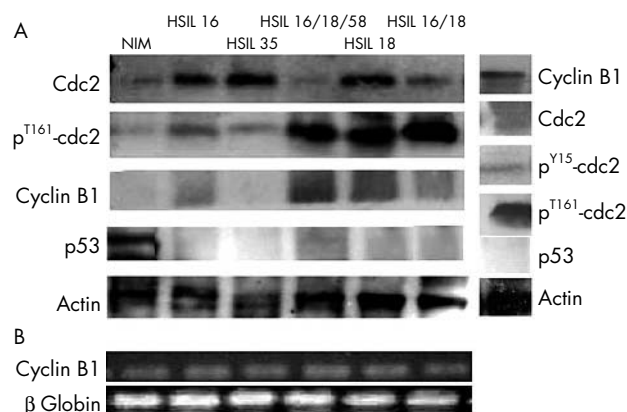


**Figure 2** Western blot analysis of cell cycle regulatory proteins, cyclin B1, cdc2, and phosphorylated cdc2 in human cervical swab samples. (A) Cdc2, T161-cdc2, and cyclin B1 were significantly upregulated in cervical lesions with human papillomavirus (HPV) infection versus normal cervical swabs. Cyclin B1 expression strongly correlated with active T161-cdc2, but not with the total amount of cdc2 (left hand panel). Cervical swab samples infected by HPV showed intense expression of cyclin B1, cdc2, and T161-cdc2 and were associated with weak expression of p53 (right hand panel). (B) This figure shows the expression of cyclin B1 transcripts. HSIL, high grade squamous intraepithelial lesion; NIM, negative for intraepithelial malignant cells.

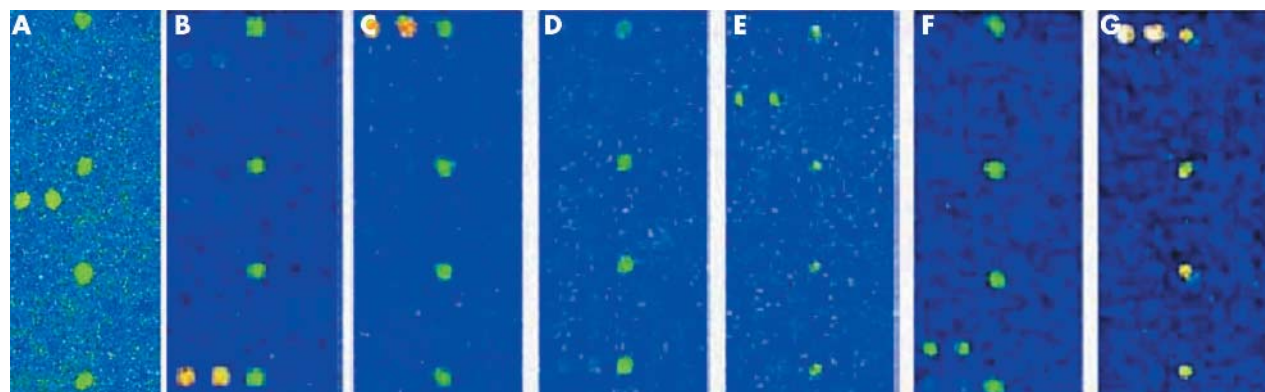


**Figure 1** The human papillomavirus (HPV) oligonucleotide microarray detected single infections using HPV probes (16/18/31/33/35/39/45/51/52/56/58/59/66/68/69). Hybridised signals were visualised using a DNA chip scanner (GSI Lumonics, ScanArray Lite, Ottawa, Canada). (A-G) The  $\beta$  globin control shows as four spots in the centre of the DNA chip, and variable HPV genotypes are noted as green signals.

1mM Na<sub>3</sub>VO<sub>4</sub>; 1mM Na<sub>5</sub>P<sub>2</sub>O<sub>7</sub>; 1mM dithiothreitol; 1mM 4-(2-amino ethyl)-benzenesulfonyl fluoride hydrochloride; 20 mg/ml leupeptin; and 20 mg/ml aprotinin). Lysates were incubated for one hour on ice (vortexed vigorously every 10 minutes) and clarified by centrifugation at 10 000 ×g for 20 minutes at 4°C. Protein concentrations were determined by the BioRad protein assay (BioRad, Hercules, California, USA). For western blot analysis, proteins were separated by Tris-glycine gel electrophoresis (Novex, San Diego, California, USA) and blotted on to a Hybond nitrocellulose membrane. Membranes were blocked for one night in PBS Tween containing 5% non-fat milk at 4°C, probed with primary antibody for 48 hours, washed three times with PBS Tween, probed again with horseradish peroxidase conjugated secondary antibody for 40 minutes, and washed three times in PBS Tween. Antigen-antibody reactions were revealed by enhanced chemiluminescence procedures according to the manufacturer's recommendations (Santa Cruz Biotechnology, Santa Cruz, California, USA). Rabbit polyclonal anti-cyclin B1 and anti-cdc2 antibodies (anti-Tyr15 phospho-cdc2; polyclonal antibody specific for residues around Tyr15 of human cdc2; and anti-Thr161 phospho-cdc2; polyclonal antibody specific for residues surrounding Thr161 of human cdc2; Cell Signaling Technology, Beverly, Massachusetts, USA) were used. Antigen-antibody complexes were visualised using the enhanced chemiluminescence detection system.

### Nuclear fractional lysis assay

To compare the relative amounts of G2 checkpoint molecules in the nuclei and the cytoplasm, a nuclear and cytoplasmic fractional lysis kit (Active Motif, Carlsbad, California, USA) was used. First, the cells were collected in ice cold PBS in the presence of phosphatase inhibitors to limit further protein modification, such as dephosphorylation or proteolysis. Next, the cells were resuspended in 0.5 ml 1 × hypotonic buffer to make them fragile by swelling the cell membrane, and then 25 µl of detergent was added to cause leakage of the cytoplasmic proteins into the supernatant. After collecting the supernatant, which made up the cytoplasmic fraction, the pellets were resuspended in 50 µl of lysis buffer in the presence of a protease inhibitor cocktail. The samples were then incubated on a rocking platform set at 150 rpm for 30 minutes at 4°C, and centrifuged at 10 000 ×g for 10 minutes

at 4°C. Finally, the supernatant was used as the nuclear fraction.

### RT-PCR

Total RNA was extracted from cervical swab and cell line samples using an Ultraspec II. Total RNA concentrations were determined by spectroscopy at 260 nm. The total RNA was then reverse transcribed into cDNA using Super Script II reverse transcriptase (Invitrogen, Carlsbad, California, USA). Total RNA (400 ng) was then mixed with 4 µl of dNTPs (2.5 mM each), 1 µl (3 µg/µl) random primers, and DEPC treated water in a total volume of 12 µl and heated to 65°C for five minutes. The samples were then mixed with 4 µl 5 × buffer, 1 µl RNase out, and heated to 42°C for two minutes. The reaction volume was then made up to 20 µl using DEPC treated water. Super Script II (1 µl) was then added and the mixture was heated to 42°C for 50 minutes and 70°C for 15 minutes. The PCR procedure was continued immediately, in the reverse RT tube, by adding 18 µl of PCR mixture to 1.5 mmol/litre MgCl<sub>2</sub>, 0.2 mmol/litre of each dNTP, 2.5 U/20 µl Taq DNA polymerase, and 20 pmol/20 µl of each primer pair of the β globin oligonucleotides. PCR amplifications began with a denaturation step of 15 minutes at 95°C and finished with an elongation step of 10 minutes at 72°C. Amplification of cDNA was performed using cyclinB1 (177 bp) primer pairs 3'-CGGGAAGTCACTGGAAACAT-5' (forward); and 3'-AAACATGGCAGTGACACCAA-5' (reverse), with 45 cycles of denaturation at 95°C for 15 minutes, annealing at 60°C for one minute, and extension at 72°C for one minute. β Globin used as a control and was amplified with the PC03/PC04 primers (PC03, 5'-ACACAACCTGTGTTCACTAGC-3'; PC04, 5'-CAACTTCATCCACGTTTAC C-3'). All the oligonucleotide primer pairs were synthesised by Bioneer Biosystems (Seoul, Korea). The PCR products (9 µl aliquots) were run on a 2.0% agarose gel in Tris buffered saline (0.05 mol/litre Tris, 0.15 mol/litre NaCl; pH 7.4) to verify the amplification efficiency, and 0.01% ethidium bromide was used for ultraviolet identification and photographic documentation.

### Colocalisation by double immunofluorescence staining

For immunofluorescence analysis, 10 µm thick paraffin wax embedded cervical tumour tissue sections were stained for cyclin B1 (Santa Cruz) and cdc2 p34 (Santa Cruz) on silane (Muto Pure Chemicals, Tokyo, Japan). Initially, the sections were dewaxed in xylene for three times 10 minutes, rehydrated through a graded ethanol series, and boiled in a microwave for seven minutes in 10mM citrate buffer (pH 6.0). Endogenous peroxidase activity was blocked by incubating in 10% normal goat serum (Zymed Laboratories Inc, South San Francisco, California, USA) in PBS for one hour at room temperature (25–28°C). The samples were incubated with anti-cyclin B1 (polyclonal) primary antibody at a dilution of 1/100 in PBS overnight at 4°C, and then with tetramethyl rhodamine isothiocyanate goat antirabbit IgG conjugated secondary antibody (Zymed Laboratories Inc) at a dilution of 1/50, for one hour at room temperature. After buffering in 10% PBS, slides were then incubated with anti-cdc2<sup>p34</sup> (monoclonal IgG against an epitope in the central domain of cdc2, amino acids 224–230) primary antibody at a dilution of 1/100 in PBS for one hour at room temperature, and then with fluorescein isothiocyanate conjugated goat antimouse IgG conjugated secondary antibody (Zymed Laboratories Inc) at a dilution of 1/50, for one hour at room temperature. Slides were then washed, mounted with anti-fade fluorescent mounting medium (Dako, Glostrup, Denmark), and then analysed by BioRad confocal microscopy.

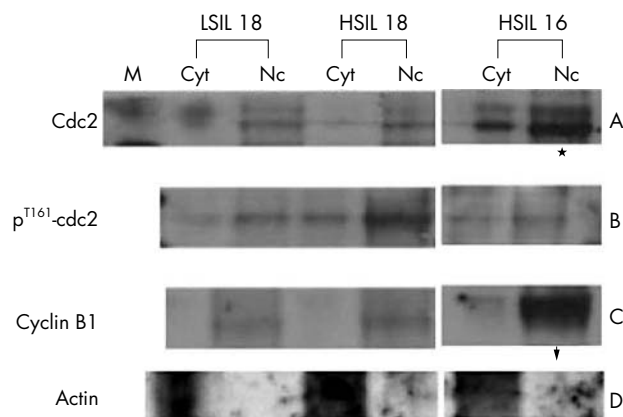


**Figure 3** Western blotting in the nuclear fractional assay for cdc2 and cyclin B1. Human cervical swab samples with human papillomavirus infection showed increased expression of cdc2, T161-cdc2, and cyclin B1, mostly in the nuclei. Cyt, cytoplasm; HSIL, high grade squamous intraepithelial lesion; LSIL, low grade squamous intraepithelial lesion; Nc, nucleus.

## Confocal three dimensional image reconstruction

### Image acquisition

Human cervical tissue specimens, including normal tissue and lesions, were obtained from the department of pathology, Yonsei University College of Medicine, Korea. They had been fixed in 10% neutral buffered formalin and were paraffin wax embedded before receipt. They were cut into 20 µm thick sections, stained with propidium iodide (PI) with RNase A (final concentration of 0.5 mg/ml), and mounted in glycerol. In addition, cytokeratin expression was analysed using indirect fluorescent immunohistochemistry (Dako; polyclonal antibody; 1/100 dilution). The cervical tissues were imaged with an MRC-1024 confocal imaging system (Biorad Microscience Ltd, Hemel Hempstead, Middlesex, UK) equipped with Axioskop microscopy (Zeiss, Thornwood, New York, USA), a 63X, 1.4 NA plan-Apochromat objective lens (Zeiss) and an Argon/Krypton laser. The fluorescent labelled antibody and PI were imaged simultaneously by using the 488 and 568 nm laser lines and collecting the emission light between 522 and 535 nm (fluorescein signal) with one photomultiplier tube and light longer than 585 nm (PI signal) with another photomultiplier tube. On confocal microscopy, a series of three dimensional optical sections, 50 nm apart, was acquired starting above the top surface of the section and extending below the bottom surface.

### Three dimensional visualisation by surface rendering

#### Mesh modelling and reconstruction

The input image was a three dimensional confocal microscope image of the fluorescent staining of the specimen. The image was composed of a stack of two dimensional images acquired at equidistant planes of 50 nm through the 20 µm sectioned specimen.

#### Smoothing

Bidirectional smoothing can subsequently be used to smooth the surface of the model in cases where there is noise or error in the data.

##### (A) Horizontal (U) direction smoothing

U direction smoothing was used to eliminate noise while conserving the original image. This method induced new point data from the area data until the unit chord length became  $\delta$ .

$$\delta = \frac{\text{Sum of chord length}}{\text{Sampling ratio} \times \text{number of points}}$$

In the case of high noise, it was preferable to produce the data with a large  $\delta$  through a small sampling rate; the sampling rate was calculated to be 0.7.

##### (B) Vertical (V) direction smoothing

Laplacian smoothing was used to eliminate noise in the vertical direction.

$$P_{new} = P_j + \lambda V_{i,j} = P_j + \lambda \sum (P_i - P_j)$$

## RESULTS

We investigated the presence of HPV DNA in 30 cervicovaginal brush samples—15 low grade squamous intraepithelial lesions and 15 high grade squamous intraepithelial lesions (HSIL)—in addition to 15 normal cervical swabs as controls, using a newly designed HPV DNA chip microarray incorporating 22 genotypes—15 high risk and seven low risk types. All cervical swab samples revealed various patterns of HPV

infection (fig 1), with eight of 30 showing multiple infections, whereas none of control samples was HPV infected. All cytological diagnoses were confirmed on biopsied tumour tissues, which comprised 15 cervical intraepithelial neoplasia grade I and 15 cervical intraepithelial neoplasia grade II–III lesions. Results, including western blot and RT-PCR in cervical swab samples, with indirect immunofluorescence and confocal image analysis in corresponding tumour tissues, are as follows.

### Aberrations in G2 checkpoint molecules

From western blot analysis of the G2 checkpoint molecules, cyclin B1 correlated well with active cdc2 (T161 phosphorylated form), but not with the total amount of cdc2, which was higher in cases with HPV infection and absence of p53 (fig 2A). Cases with HPV infection showed intense expression of cyclin B1 and the active form of cdc2 (T161 phosphorylated cdc2). The expression of cyclin B1 protein was higher in cases of HPV infection, whereas cyclin B1 transcripts appeared to be expressed ubiquitously when assessed by RT-PCR (fig 2B).

The nuclear fractional assay revealed that the expression of both molecules—cdc2 and cyclin B1—was higher in the nuclei than in the cytoplasm (fig 3).

Confocal microscopy based double immunofluorescence using FITC (green) conjugated anti-cdc2 monoclonal antibody and TRITC (red) conjugated anti-cyclin B1 polyclonal antibody revealed an abrupt transition between HSIL and the normal epithelium. HSIL showed strong positivity for both cyclin B1 and cdc2, whereas the normal epithelium was negative for both (fig 4A). The cyclin B1–cdc2 complex was strongly expressed in the whole squamous epithelium in HSIL, and cyclin B1 was seen even in the superficial layer, whereas cdc2 was found predominately in the parabasal and intermediate layers (fig 4B). Cyclin B1 predominated in the nuclei of the upper squamous epithelium, whereas cdc2 was found in both the nuclei and the cytoplasm (fig 4C). Cdc2 and cyclin B1 were colocalised in the nuclei of the lower squamous epithelium in HSIL (fig 4D).

### Three dimensional visualisation

Volume rendering and surface rendering methods were used to produce a three dimensional reconstruction from stacks of two dimensional confocal images. On visualisation of the cytoplasm, texture based volume rendering was used as appropriate. On analysis of two dimensional stacking image files by the conversion of video images, koilocytes of the uterine cervical squamous epithelium that appeared to be binucleated were shown to be gradually conjoined to one another by an anaphase bridge (fig 5A), and were finally proved to be multilobated, single nuclei. Even multinucleated cells that appeared to be completely separated when viewed under conventional two dimensional microscopy were eventually revealed to be single, fused nuclei (fig 5B).

## DISCUSSION

HPV infection may lead to altered phenotypes in addition having effects on cell biology that have important clinical consequences in the uterine cervix. Extensive studies have been conducted with regard to cell cycle alteration during HPV infection, particularly in terms of p53 abrogation.<sup>15 16</sup> Recently, the G2 and G1 checkpoints have also been shown to be aberrant,<sup>10 17–20</sup> even though the mechanisms involved are unknown. However, there are few studies that connect cell biology with phenotypic alteration in cervical epithelial cells infected by HPV, the so called koilocytes.

In our present study, the expression of cyclin B1 protein in various clinical samples showing HPV infection was variable, even in terms of the ubiquitous expression of cyclin B1 mRNA. Increased cyclin B1 was associated with T161-cdc2,

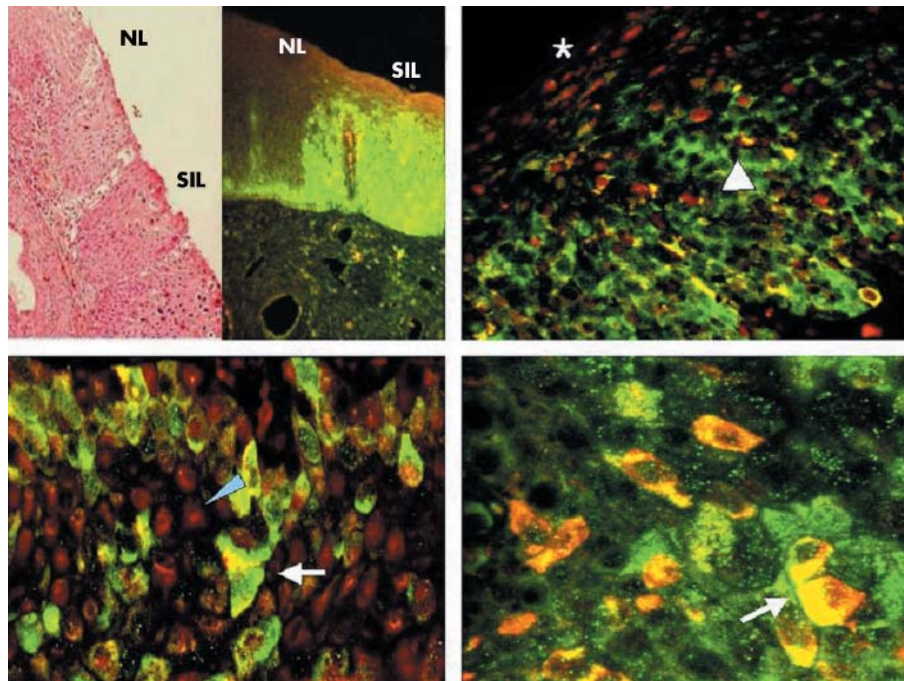


**Figure 4** Confocal based dual immunofluorescence of cyclin B1 and cdc2 in high grade squamous intraepithelial lesions (HSIL) with human papillomavirus infection. The red signal shows labelling with TRITC conjugated goat antirabbit IgG antibody/cyclin B1 polyclonal primary antibody, and the green signal shows labelling with FITC conjugated goat antimouse IgG antibody/cdc2 monoclonal antibody. (A) Abrupt transition between the normal epithelium and HSIL (left, haematoxylin and eosin staining; right, immunofluorescent staining; original magnification, both  $\times 40$ ). (B) Merged view of the cyclin B1–cdc2 complex in the squamous epithelium of HSIL. Cyclin B1 is seen even in the superficial layer (asterisk), whereas cdc2 is seen mainly in the parabasal and intermediate layers (arrowhead) (original magnification,  $\times 100$ ). (C) Cyclin B1 was seen predominantly in the nuclei (arrowhead), and cdc2 in both nuclei and cytoplasm in the upper layer of the squamous epithelium. Note the yellow signals showing the colocalisation of cyclin B1 and cdc2 in both the nuclei and the cytoplasm (arrow) (original magnification,  $\times 200$ ). (D) Higher magnification of the colocalisation of cdc2 and cyclin B1 (arrow) in lower squamous epithelium (original magnification,  $\times 460$ ).

but not with total cdc2, in cases of HPV infection. However, Y15-cdc2 (inactive form of cdc2) expression was not specific to HPV genotypes, but was specific to disease progression. In normal cytological samples and low grade squamous intraepithelial lesions, Y15-cdc2 was the major form of cdc2. T161-cdc2 was detected only in cases infected by high risk HPV, irrespective of the grade of the lesion. Entry of all eukaryotic cells into the M phase of the cell cycle is regulated by the activation of cdc2 kinase, and the catalytic activity of cellular cdc2 and cyclin B is primarily regulated at the post-translational level. The activation of cdc2 is controlled at several steps, including cyclin binding and the phosphorylation of T161.<sup>10–17–18</sup> However, the crucial regulatory mechanisms involved in progression into mitosis are the phosphorylation of Y15 and consequent inactivation of cdc by Wee1 and Myt1 protein kinases, and the dephosphorylation of Y15 and consequent activation of cdc2 by cdc25 phosphatase.<sup>17–19</sup> T161 phosphorylation may be more stable than phosphorylation at T14 and Y15.<sup>9</sup> During the normal cell cycle, phosphorylation of T161 tends to rise and fall in parallel with cyclin binding. Because both the T161-cdc2 and cyclin B1 proteins were increased only in HPV infected cases, the increased activity of cdc2 through the phosphorylation of T161 associated with HPV infection, together with binding to cyclin B1 protein, may abrogate the G2 checkpoint.

Although the mechanisms involved in cyclin B1 regulation are not fully understood, recent evidence shows that p53 regulates the G2 checkpoint not only by attenuating the activity of the cyclin B1 promoter,<sup>15</sup> but also by binding to the cell cycle regulating kinase p34<sup>cdc2</sup>.<sup>16</sup> Our finding that cyclin B1 and the active form of cdc2 are significantly upregulated only in cases of HPV infection suggests that this upregulation may provide an additional mechanism of abrogating the G2

checkpoint. In conclusion, HPV E6 decreases the fidelity of mitotic checkpoints and increases cdc2 functional activity, leading to chromosomal instability and mitotic checkpoint arrest. Therefore, it is not surprising that what appear to be multiple nuclei in one koilocyte are in fact multilobation of a single nucleus caused by unfinished nuclear division. Multinucleation has traditionally been regarded as one of the most distinctive features of koilocytes, but we suspect that these features are caused by the limited two dimensional view of koilocytes seen by conventional microscopy. Confocal three dimensional reconstruction is a powerful technology to detect constitutional cytomorphology that is beyond the limitations of classic light microscopy.

“Multinucleation has traditionally been regarded as one of the most distinctive features of koilocytes, but we suspect that these features are caused by the limited two dimensional view of koilocytes seen by conventional microscopy”

In general, visualisation on the basis of cell volume data uses methods of surface and volume rendering.<sup>21–26</sup> With the use of a DNA PI probe in combination with an anti-cytokeratin antibody, it has been shown that the nuclear shapes of dysmorphic cells can be clearly visualised in three dimensions. First, viewing a series of confocal images visually identifies the cell of interest, such as a koilocyte. Next, the cell of interest is segmented based on label intensity and morphology. Using the labelvoxel module, the contours of the koilocytes in several key frames are first outlined, and then the contours in every section are automatically demarcated with the interpolate function. Next, a series of demarcated

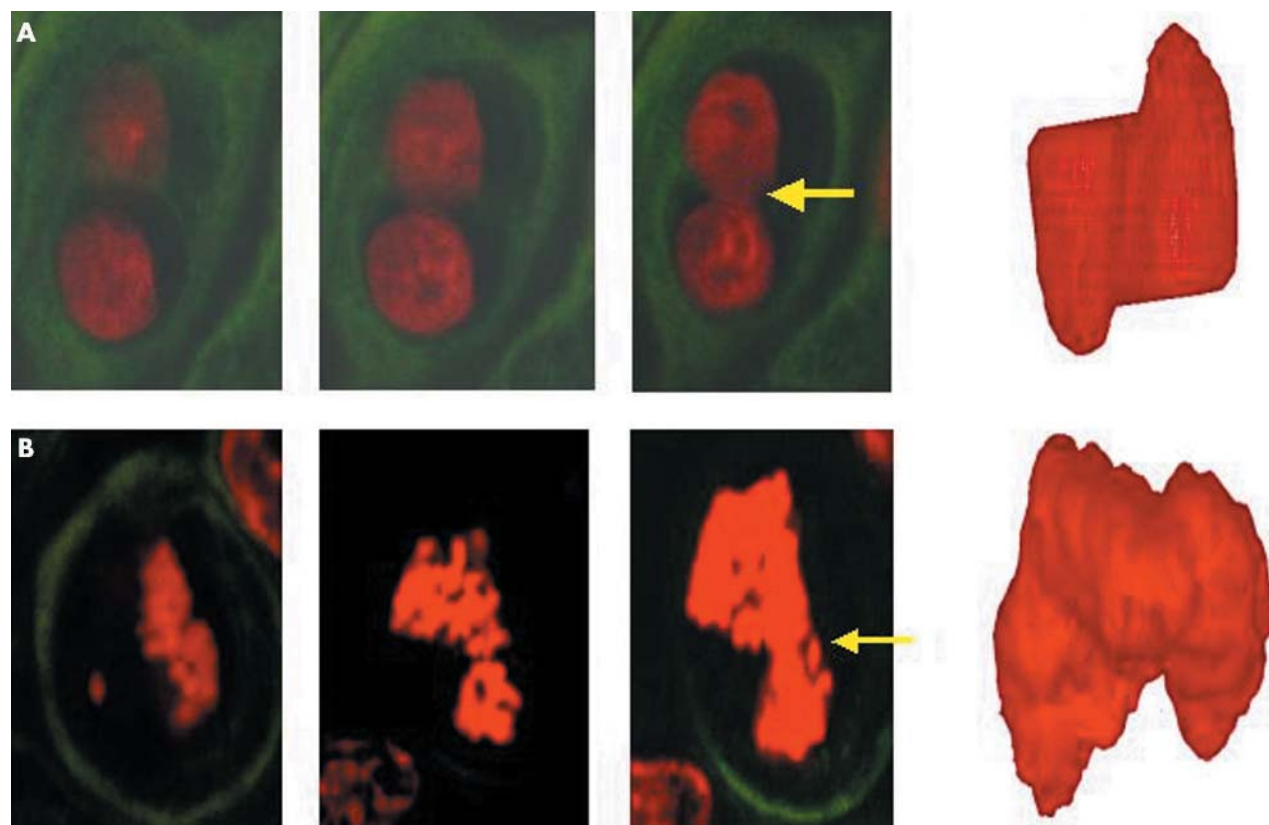


**Figure 5** Serial views of koilocytes using three dimensional reconstruction and surface rendering. (A) Binucleation with a perinuclear cavity characteristic of a koilocyte revealed a single, central, fused, bilobated nucleus. Surface and wire frame rendering showed bilobation connected by an anaphase bridge (arrow). (B) An extremely irregular multinucleated nucleus was shown be a single multilobated nucleus (arrow). On surface rendering magnification, its contour was too notched to be multinucleated in the two dimensional plane.

contours is used as a template to extract the cell of interest using the arithmetic function. The segmented koilocytes can then be visualized using several, different three dimensional modes. To retain the information on differences in signal intensities, the vortex module is applied. The resulting three dimensional image can be rotated to any viewing angle. This function is highly valuable for observing cells with irregular contours. Alternatively, surface rendering is applied when the intensity is not so important as processing only surface voxels. The resulting three dimensional images show only binary information on the surface texture. We adopted a texture based volume rendering module after skinning and the application of a loft algorithm for the mesh model. Next, the “U” and “V” direction smoothing algorithm was used to smooth the demarcated contour. For high quality magnification of selected cells, subdivision was performed using a loop algorithm.

A three dimensional reconstruction of the complete cytomorphology of cytopathic changes as a consequence of

HPV infection showed that multinucleation specific to koilocytes is in fact the result of non-division of a multilobated single nucleus. Even koilocytes that appeared to be binucleated using conventional two dimensional microscopy were shown to contain multilobated single nuclei. In these cells, HPV oncoproteins and chromosomal instability associated with G2 checkpoint aberrations, together with abrogated p53 expression, result in the accumulation of genetic instability with the subsequent formation of a non-dividing, multilobated nucleus.

In conclusion, our results show that the apparent multiple nuclei of koilocytes are an artefact of two dimensional observations. The apparent multinucleation of a single koilocyte nucleus was recognised by three dimensional confocal reconstruction analysis, and is caused by upregulation of gene products related to the G2 checkpoint in these cells compared with normal epithelial cells.

**ACKNOWLEDGEMENTS**

This study was supported by BK21 project for medical science, Yonsei University College of Medicine and 2002 Goog Health R&D projects, Ministry of Health and Welfare, Korea (NHC, GBJ, HKC).

**Authors’ affiliations**

**N H Cho, S Kang, S Hong**, Department of Pathology, Seodaemun-ku, Sinchon-dong 134, Yonsei University College of Medicine, 120-752, Seoul, Korea  
**G B Jeong**, Department of Anatomy, Chungbuk Medical University, Chungju City, 364-763, Chungbuk Province, Korea  
**I W Choi, H J Choi, H K Choi**, Department of Computer Engineering, Inje University, 621-749, Pusan, Korea

**Take home messages**

- The apparent multiple nuclei of koilocytes are an artefact of two dimensional observations, which were shown by three dimensional confocal reconstruction analysis to be multilobation of a single nucleus
- This phenomenon is thought to be caused by upregulation of gene products related to the G2 checkpoint, such as cyclin B1 and active cdc2

## REFERENCES

- 1 **Vooijs GP**. Benign proliferative reaction, intraepithelial neoplasia, and invasive cancer of the uterine cervix. In: Bibbo M, ed. *Comprehensive cytopathology*, 2nd ed. Philadelphia: WB Saunders, 1997:161–230.
- 2 **Herrington S**. The pathogenesis of cervical neoplasia. In: Gray W, McKee GT, eds. *Diagnostic cytopathology*, 2nd ed. London: Churchill Livingstone, 2003:707–53.
- 3 **Hummel M**, Hudson JB, Laimins LA. Differentiation-induced and constitutive transcription of human papillomavirus type 31 in cell lines containing viral episomes. *J Virol* 1992;**66**:6070–80.
- 4 **Lambert PF**. Papillomavirus DNA replication. *J Virol* 1991;**65**:3417–20.
- 5 **Doorbar JC**, Foo N, Coleman L, et al. Characterization of events during the late stage of HPV 16 infection in vivo using high affinity synthetic FAbs to E4. *Virology* 1997;**238**:40–52.
- 6 **Ruesch MN**, Laimins LA. Human papillomavirus oncoproteins after differentiation-dependent cell cycle exit on suppression in semisolid medium. *Virology* 1998;**250**:19–29.
- 7 **Fratini MG**, Lim HB, Laimins LA. In vitro synthesis of oncogenic human papillomavirus requires episomal genomes for differentiation-dependent late expression. *Proc Natl Acad Sci U S A* 1996;**93**:3062–7.
- 8 **Krek W**, Nigg EA. Differential phosphorylation of vertebrate p34cdc2 kinase at the G1/S and G2/M transitions of the cell cycle: identification of major phosphorylation sites. *EMBO J* 1991;**10**:305–16.
- 9 **Norbury C**, Blow J, Nurse P. Regulatory phosphorylation of the p34cdc2 protein kinase in vertebrates. *EMBO J* 1991;**10**:3321–9.
- 10 **Thompson DA**, Belinsky G, Chang THT, et al. The human papillomavirus-16 E6 oncoprotein decreases the vigilance of mitotic checkpoints. *Oncogene* 1997;**15**:3025–35.
- 11 **Duensing S**, Lee LY, Duensing A, et al. The human papillomavirus type 16 E6 and E7 oncoproteins cooperate to induce mitotic defects and genomic instability by uncoupling centrosome duplication from the cell division cycle. *Proc Natl Acad Sci U S A* 2000;**97**:10002–7.
- 12 **Duensing S**, Duensing A, Crum CP, et al. Human papillomavirus type 16 E7 oncoprotein-induced abnormal centrosome synthesis is an early event in the evolving malignant phenotype. *Cancer Res* 2001;**61**:2356–60.
- 13 **Duensing S**, Munger K. The human papillomavirus type 16 E6 and E7 oncoproteins independently induce numerical and structural chromosome instability. *Cancer Res* 2002;**62**:7075–82.
- 14 **Thomas J**, Laimins LA. Human papillomavirus oncoproteins E6 and E7 independently abrogate the mitotic spindle checkpoint. *J Virol* 1998;**72**:1131–7.
- 15 **Innocente SA**, Abrahamson JLA, Cogswell JP, et al. P53 regulates a G2 checkpoint through cyclin B1. *Proc Natl Acad Sci U S A* 1999;**96**:2147–52.
- 16 **Ababneh M**, Gotz C, Montenarh M. Downregulation of the cdc2/cyclin B protein kinase activity by binding of p53 to p34<sup>cdc2</sup>. *Biochem Biophys Res Commun* 2001;**283**:507–12.
- 17 **Southern SA**, McDicken IW, Herrington CS. Evidence for keratinocyte immortalization in high-grade squamous intraepithelial lesions of the cervix infected with high-risk human papillomavirus. *Lab Invest* 1999;**80**:539–44.
- 18 **Atherton-Fessler S**, Parker LL, Geahlen RL, et al. Mechanisms of p34cdc2 regulation. *Mol Cell Biol* 1993;**13**:1675–85.
- 19 **Watanabe N**, Broome M, Hunter T. Regulation of the human WEE1Hu CDK tyrosine 15-kinase during the cell cycle. *EMBO J* 1995;**14**:1878–91.
- 20 **McGowan CH**, Russell P. Human Wee1 kinase inhibits cell division by phosphorylating p34cdc2 exclusively on Tyr15. *EMBO J* 1993;**12**:75–85.
- 21 **Liu Y**, Chiang A. High-resolution confocal imaging and three-dimensional rendering. *Methods* 2003;**30**:86–93.
- 22 **Strohmaier A**, Porwol T, Acker H, et al. Three-dimensional organization of microtubules in tumor cells studied by confocal laser scanning microscopy and computer-assisted deconvolution and image reconstruction. *Cells Tissues Organs* 2000;**167**:1–8.
- 23 **Solorzano COD**, Rodriguez EG, Jones A, et al. Segmentation of confocal microscope images of cell nuclei in thick tissue sections. *J Microsc* 1999;**193**:212–26.
- 24 **Lockett SJ**, Sudar S, Thompson CT, et al. Efficient interactive and three-dimensional segmentation of cell nuclei in thick tissue sections. *Cytometry* 1998;**31**:275–86.
- 25 **Adiga U**. Integrated approach for segmentation of 3-D confocal images of a tissue specimen. *Microsc Res Tech* 2001;**54**:260–70.
- 26 **Lin G**, Adiga U, Olson K, et al. A hybrid 3D watershed algorithm incorporating gradient cues and object models for automatic segmentation of nuclei in confocal image stacks. *Cytometry* 2003;**56**:23–36.



## Multinucleation of koilocytes is in fact multilobation and is related to aberration of the G2 checkpoint

N H Cho, S Kang, S Hong, et al.

*J Clin Pathol* 2005 58: 576-582  
doi: 10.1136/jcp.2004.022152

---

Updated information and services can be found at:  
<http://jcp.bmj.com/content/58/6/576.full.html>

- 
- These include:*
- References** This article cites 24 articles, 9 of which can be accessed free at:  
<http://jcp.bmj.com/content/58/6/576.full.html#ref-list-1>
- Article cited in:  
<http://jcp.bmj.com/content/58/6/576.full.html#related-urls>
- Email alerting service** Receive free email alerts when new articles cite this article. Sign up in the box at the top right corner of the online article.

- 
- Topic Collections** Articles on similar topics can be found in the following collections
- [Cervical cancer](#) (68 articles)
  - [Gynecological cancer](#) (150 articles)
  - [Immunology \(including allergy\)](#) (1279 articles)

---

### Notes

---

To request permissions go to:  
<http://group.bmj.com/group/rights-licensing/permissions>

To order reprints go to:  
<http://journals.bmj.com/cgi/reprintform>

To subscribe to BMJ go to:  
<http://group.bmj.com/subscribe/>